

Stabilization of a Two-Wheeled Mobile Pendulum System using LQG and Fuzzy Control Techniques

Ákos Odry, Péter Odry

Dept. of Control Engineering and Information Technology
University of Dunaújváros
Dunaújváros, Hungary
E-mail: odrya@mail.duf.hu, podry@mail.duf.hu

János Fodor

Institute of Intelligent Engineering Systems
Óbuda University
Budapest, Hungary
E-mail: fodor@uni-obuda.hu

Abstract—This paper studies the control performances of modern and soft-computing based control solutions. Namely, the stabilization of a naturally unstable mechatronic system will be elaborated using linear-quadratic-Gaussian and cascade-connected fuzzy control schemes. The mechatronic system is a special mobile robot (so called two-wheeled mobile pendulum system) that has only two contact points with the supporting surface and its center of mass is located under the wheel axis. Due to this mechanical structure, the inner body (which acts as a pendulum between the wheels) tends to oscillate during the translational motion of the robot, thus the application of feedback control is essential in order to stabilize the dynamical system. In the first part of the paper, the mechatronic system and the corresponding mathematical model are introduced, while in the second part the aforementioned control solutions are designed for the plant. The achieved control performances are analyzed both in simulation environment and on the real mechatronic system. At the end of the paper, a performance assessment of the elaborated control solutions is given based on transient response and error integral measurements.

Keywords—Fuzzy control; LQG control; Kalman filter; mobile robot; self-balancing robot; future transportation system

I. INTRODUCTION

Nowadays, technological developments face dynamical systems that are getting more and more complex and complicated by the day. These complex systems are characterized by high order dynamics, uncertain parameters, and most often, their nonlinear mathematical model is only approximately known (such as the analyzed system in the INTELLI 2015 paper [1]). Over the last few decades, we have seen that conventional and modern linear control techniques have been extensively applied in control development and industrial automation, however, their performance is always questioned, when systems with uncertainty and unmodeled dynamics are controlled. In general, these linear controllers do not work well for nonlinear vague systems [2]. On the other hand, Zadeh's fuzzy logic and reasoning introduced a new control perspective, where imprecision and uncertainty form the basis of the inference mechanism [3]. Fuzzy logic control plays an important role in systems with unknown structure, and it has been widely used in automotive control applications. Thanks to its rapid progress, fuzzy reasoning is a fruitful research area for the Robotics and Control Community, where the achievable control performance and

competitive control solutions are continuously investigated [4]. This paper studies the control performance of linear-quadratic-Gaussian and fuzzy control techniques.

The linear-quadratic-Gaussian (LQG) technique is a beloved method in the control of dynamical systems since it provides the optimal state feedback gain based on the well-developed mathematical algorithm [5]. Numerous researches have been dealt with its application and control performance in real embedded environments. Divelbiss and Wen [6] presented their experimental results of the tracking control of a car-trailer system, where linear quadratic regulator was used to track the trajectory. Ji and Sul [7] proposed an LQG-based speed control method for torsional vibration suppression in a 2-mass motor drive system, which gave satisfying performance and robust behavior against parameter variations. Recent efforts broaden further the set of experimental research results regarding the LQG control, including the control of inverted pendulum type assistant robot [8], self-balancing unicycle robot [9], unmanned helicopter in an uncertain environment [10], and quadrotor UAVs [11] as well.

On the parallel thread, fuzzy logic control has also proved its competitive performance. Due to the provided flexibility and smoothness in the control action, and the linguistic information based design technique as well, it is applied more and more in dynamical systems. McLean and Matsuda [12] designed a fuzzy logic controller, which provided acceptable station-keeping performance for a single main rotor helicopter even in severe turbulences. Das and Kar [13] proposed adaptive fuzzy controllers for the robust control of nonholonomic mobile robots that were characterized with uncertain parameters. Lee and Gonzalez [14] examined the achieved control performance of the conventional PID and fuzzy techniques for position control of a muscle-like actuated arm. Moreover, fuzzy control was successfully applied in the development area of walking robots as well. Kecskés and Odry [15] elaborated the optimized fuzzy control of a hexapod walking robot called Szabad(ka)-II. Finally, fuzzy logic based stabilization of two-wheeled inverted pendulum systems has also been investigated both in simulation environment and on the real plant [17]. Many applications have been proposed where fuzzy control showed superior performance (such as [12], [15]), however, the opposite outcome was often claimed as well (such as in [14]). Therefore, the effective and

beneficial applicability of fuzzy control still remains an important issue to be further addressed.

The objective of this paper is to make an analysis, and give a comparative assessment regarding the achieved control performances of both control techniques. The robustness of the elaborated controllers will also be investigated using the simulation and measurement results. The controlled plant is a two wheeled mobile pendulum system [18] (hereinafter robot), whose dynamics is highly nonlinear, moreover, its mathematical model is characterized by uncertain parameters (the model has not been validated). It will be discussed what is the influence of the uncertain dynamics, and how it affects the achieved closed loop behavior of the real robot. The stabilization of the plant with the LQG technique has been investigated in [1], while in [19] a fuzzy control scheme has been designed. This paper summarizes the results of [1] and [19], and based on the evaluation of different step responses (where both the simulation and measurement results will be taken into account), the better control strategy will be identified. For the comparative assessment different error integrals (as quality measurement numbers) will be evaluated.

The remainder of this paper is organized as follows. In Section II, the mechatronic structure of the robot is introduced, while in Section III, the corresponding nonlinear mathematical model is derived. In Section IV, the control task and the LQG and fuzzy control techniques are reviewed. Section V deals with the elaboration of the LQG control strategy, while Section VI describes the applied fuzzy control scheme. The simulation and implementation results of the elaborated control strategies are given in Sections VII and VIII, respectively. Section IX describes the comparative assessment based on the simulation and measurement results, while Section X contains the conclusions and the future work recommendations.

II. THE FABRICATED MECHATRONIC SYSTEM

The mechatronic system is a special mobile robot (so called two-wheeled mobile pendulum system) that consists of two wheels and a steel inner body (chassis). The wheels are actuated through DC motors attached to the body. As it can be seen in Figure 1, the diameter of the wheels is bigger than the



Figure 1. Photograph of the fabricated robot.

TABLE I. THE APPLIED SENSORS IN THE EMBEDDED ELECTRONICS

Sensor	Manufacturer	Type
Accelerometer	STMicroelectronics	LIS331DL
Gyroscope	STMicroelectronics	L3G4200D
Current sensors	Texas Instruments	INA198
Incremental encoders	Faulhaber	PA2-100

diameter of the intermediate body, thus the robot has only two contact points with the supporting surface. Due to this mechanical structure, the inner body behaves as a pendulum between the stator and rotor of the applied DC motors, and tends to oscillate when the robot performs translational motion.

Since the location of the center of mass of the robot can be under and above the wheel axis, two equilibrium points can be distinguished. Namely, the robot stays around its stable equilibrium point when the center of mass is located under the wheel axis. Therefore, around this state the translational motion of the robot is affected by the damped oscillation of its inner body. On the other hand, the robot is operated around its unstable equilibrium point when the center of mass is stabilized above the wheel axis. Around the unstable equilibrium point, the robot simultaneously performs translational motion and balances its inner body, which acts as an inverted pendulum. For video demonstration see the website [20].

The electronic construction is built around two 16-bit ultra-low-power Texas Instruments MSP430F2618 microcontrollers (hereinafter MCU1 and MCU2). The applied sensors are summarized in Table I. The actuators are 3V geared DC micromotors (type: 1024N003S) manufactured by Faulhaber. The motors are driven with pulse width modulation (PWM) signals through Texas Instruments DRV592 drivers. The electronic system is supplied from stabilized 3.3V, the source is a 1 cell lithium-polymer (Li-Po) battery. A 16 MHz quartz oscillator is used as the system clock.

Similar construction was built at the McGill University's Centre for Intelligent Machines [21]. It was proven that the two contact point construction is characterized by the so called quasiholonomic property that eases the control of nonholonomic systems. Another corresponding two contact point construction is the electric Diwheel built by the School of Mechanical Engineering at the University of Adelaide [22].

III. MATHEMATICAL MODEL

To be able to efficiently design the control algorithms of the system, its mathematical model has to be obtained first. Most of the electrical and mechanical parameters that characterize the robot dynamics (such as wheel radius or resistance of the motor) are quite accurately known from direct measurements, datasheets or from calculations performed by Solidworks, the rest of the parameters were experimentally tuned based on the measurements.

We indicate with θ_1 and θ_2 the angular displacements of the wheels, while with θ_3 the inclination angle of the

pendulum (inner body). The parameters that characterize the robot are summarized in Table VI in the appendix. The following notations will also be used: $\sigma = \dot{\psi}$ as the yaw rate of the robot, and $\nu = \dot{s}$ as the linear speed of the robot, i.e., $\dot{\psi} = r(\dot{\theta}_2 - \dot{\theta}_1)/d$, and $\dot{s} = r(\dot{\theta}_1 + \dot{\theta}_2)/2$.

The motion of the system was determined by the help of the Lagrange equations [23], which lead us to the following equations of motion of the mechanical system [18]:

$$M(q)\ddot{q} + V(q, \dot{q}) = \tau_a - \tau_f, \quad (1)$$

where $M(q)$ denotes the 3-by 3 symmetric and positive definite inertia matrix, $V(q, \dot{q})$ denotes the 3-dimensional vector term including the Coriolis and centrifugal force terms and also the potential (gravity) force term. The Lagrange function and the exact elements of the matrices in (1) are described in the appendix. For the vector of generalized coordinates $q = (\theta_1, \theta_2, \theta_3)^T$ was chosen, since it contains the minimum number of independent coordinates that define the configuration of the system. The generalized external forces in (1) consist of the torques τ_a that are produced by the motors and the effect of friction τ_f that is modeled in the system [18]. The torques τ_a are described by the differential equation (2), where the input voltages and currents of the motors are denoted with $u = (u_1, u_2)^T$ and $I = (I_1, I_2)^T$.

$$\begin{aligned} i &= \frac{1}{L} \left(u - k_E k \begin{bmatrix} 1 & 0 & -1 \\ 0 & 1 & -1 \end{bmatrix} \dot{q} - RI \right) \\ \tau_a &= k_M k \begin{bmatrix} 1 & 0 \\ 0 & 1 \\ -1 & -1 \end{bmatrix} I \end{aligned} \quad (2)$$

Regarding the effect of friction τ_f , only viscous frictions were assumed. Namely, viscous friction was modelled at the bearings and between the wheels and the supporting surface:

$$\tau_f = \begin{bmatrix} b + f_v & 0 & -b \\ 0 & b + f_v & -b \\ -b & -b & 2b \end{bmatrix} \dot{q}. \quad (3)$$

Based on (1) the state-space representation of the two-wheel inverted pendulum system is obtained. With the state vector $x = (q, \dot{q}, I)^T$ the state-space equation is [18]:

$$\begin{aligned} \dot{x}(t) &= h(x, u), \\ h(x, u) &= \begin{bmatrix} \dot{q} \\ M(q)^{-1} (\tau_a - \tau_f - V(q, \dot{q})) \\ \frac{1}{L} (u - k_E k \begin{bmatrix} 1 & 0 & -1 \\ 0 & 1 & -1 \end{bmatrix} \dot{q} - RI) \end{bmatrix}, \quad (4) \\ y(t) &= x(t). \end{aligned}$$

Remark: In the simulation environment the state-space equation (4) was implemented, however, during the design of the LQG controllers the 6-dimensional version defined by the

state vector $x = (q, \dot{q})^T$ was used. This outcome was chosen because the current measurements were that noisy that the states $I = (I_1, I_2)^T$ could not be used in the feedback. The 6-dimensional model is derived by neglecting the inductance L of the motors.

IV. THE CONTROL TASK

The anti-sway speed control of the robot was investigated in the analysis, e.g., such control strategies have been elaborated, which simultaneously minimize the oscillations (around the stable equilibrium point) of the inner body and ensures the translational motion of the robot:

- $\lim_{t \rightarrow \infty} \dot{s}(t) = \nu_d$ for the linear speed of the robot,
- $\lim_{t \rightarrow \infty} \dot{\psi}(t) = \sigma_d$ for the yaw rate of the robot,
- $\lim_{t \rightarrow \infty} \dot{\theta}_3(t) = 0$ for the oscillation of the inner body,

where ν_d and σ_d denote the desired values of the linear speed and yaw rate of the robot, respectively. In the following subsections, the applied control techniques and the elaboration procedures are reviewed.

A. LQ control

The linear-quadratic control addresses the issue of achieving a balance between good system response and control effort [5]. It is based on a developed mathematical algorithm, which results the optimal state-feedback gain K . The feedback gain K minimizes the quadratic cost function

$$J(x, u) = \frac{1}{2} \sum_{k=0}^{N-1} (x_k^T Q x_k + u_k^T R u_k) + \frac{1}{2} x_N^T Q x_N, \quad (5)$$

where $x \in \mathbb{R}^n$ and $u \in \mathbb{R}^m$ are the state and input of the system described by its state-space equation, while $Q = Q^T \in \mathbb{R}^{n \times n}$, $Q \geq 0$ and $R \in \mathbb{R}^{m \times m}$, $R > 0$ are weighting matrices. According to the LQ method, the state feedback matrix is given by $K = (R + B^T P B)^{-1} B^T P A$, where $P = P^T \geq 0$ is the unique solution of the Control Algebraic Riccati Equation (CARE). The optimal state-feedback $u_k = -K x_k$ ensures the asymptotic stability of the closed loop system. The feedback matrix K is calculated by the built-in Matlab function `lqr(A,B,Q,R,Ts)`. Since the LQ control defined by the objective function (5) drives the system from the initial state x_0 to the state $x_d = 0$, the control structure shall be extended with the reference tracking matrices:

$$\begin{pmatrix} N_x \\ N_u \end{pmatrix} = \begin{bmatrix} A - I & B \\ C & 0 \end{bmatrix}^{-1} \begin{pmatrix} 0_{n \times m} \\ I_m \end{pmatrix}, \quad (6)$$

where 0 and I are the zero and identity matrices, respectively (the sizes are given in the subscript).

B. Kalman filtering

In the development of the optimal LQ control strategy it is assumed that the state variables are measurable, and the system is not disturbed by either internal or external noises.

However, in practice, the opposite situation is quite common, namely, that a part of the state vector is too noisy to be used directly in the feedback. The LQG strategy provides optimal control gain to stochastic, noisy systems by minimizing the expected value of the quadratic objective function (5).

Based on the separation principle the LQG control strategy is given by the state-feedback $u_k = -K\hat{x}_k$, where K is the optimal control gain determined by the LQ algorithm, while \hat{x}_k state vector consists of the original states (those states of x_k that were not noisy) and the Kalman filter based estimation of the noisy states. Let us denote the unmeasurable or noisy states with ξ , then the corresponding noisy linear system can be given as:

$$\begin{aligned}\xi_{k+1} &= \Phi\xi_k + \Gamma\rho_k + w_k, \\ \gamma_k &= P\xi_k + z_k,\end{aligned}\quad (7)$$

where the process and measurement noises are indicated with w and z , respectively, and according to the stochastic hypothesis these noises are uncorrelated and their mean value is zero. In this case the Kalman filter algorithm provides the optimal estimation $\hat{\xi}$ of the state ξ , i.e., $E[\xi_k - \hat{\xi}_k] = 0$ and $E[(\xi_k - \hat{\xi}_k)(\xi_k - \hat{\xi}_k)^T] \rightarrow \inf$. The estimation algorithm can be found in [24].

Therefore, the design steps of the LQG control strategy are the following: i.) Linearization of the mathematical model around an equilibrium point, ii.) Controllability analysis, iii.) Specification of the weighting matrices, iv.) Calculation of the optimal control gain K , v.) Identification of the noisy states, vi.) Specification of the noise covariance parameters of the filter, vii.) State estimation by Kalman filter and viii.) Application of the state feedback strategy $u_k = -K\hat{x}_k$.

C. Fuzzy control

Lofti A. Zadeh introduced the fuzzy sets [3] by extending the classical two-valued logic $\{0,1\}$ with the whole continuous interval $[0,1]$. Fuzzy reasoning is based on the application of these fuzzy sets, which result that the inference mechanism of a fuzzy logic controller is defined by simple IF-THEN linguistic rules. Hence, there is no need to define certain models, instead the empirical rules and the approximate reasoning lead to a heuristically defined control strategy. The algorithm is composed of the following parts [25].

- Fuzzification: Mapping the available crisp measurements to the fuzzy interval $[0,1]$. The fuzzy interval describes the membership of the fuzzy input variable. The membership function of a fuzzy set A is denoted with $\mu_A(x) \in [0,1]$, where x is the crisp measurement.
- Inference machine: The fuzzy IF-THEN rules define the implication relation between the antecedents and consequents. The inference mechanism consists of assigning the so-called firing level to the output fuzzy set defined in each rule. The firing level represents the result of the antecedent evaluation. The aggregation procedure is the last part of the inference machine, where the output

fuzzy sets are combined into a single fuzzy set (overall fuzzy output is calculated).

- Defuzzification: Mapping back the output fuzzy set to crisp domain. The most popular defuzzification methods are the center of gravity and the weighted average method [25].

The concrete elaboration procedure (e.g., selecting the fuzzy sets and fuzzy rules, defining the inference mechanism, and applying the defuzzification method as well) will be described in Section VI.

V. ELABORATION OF THE LQG CONTROL STRATEGY

The goal of the elaboration is to calculate the optimal state feedback and reference tracking matrices that drive the motors such a way that both the speed control of the robot and the suppression of the inner body oscillations are ensured.

A. Optimal state feedback

The linear state space equation is given by the linearization of (4) around the equilibrium $(x_e, u_e) = (0,0)$:

$$\dot{x} = \underbrace{\left(\frac{\partial h}{\partial x}\right)}_{A_s(x_e, u_e)} x(t) + \underbrace{\left(\frac{\partial h}{\partial u}\right)}_{B_s(x_e, u_e)} u(t), \quad (8)$$

where the subscript s refers to the stable equilibrium point. In order to reduce the complexity of implementation the $\tilde{x} = Tx = (s, \theta_3, \dot{s}, \dot{\theta}_3, \psi, \dot{\psi})$ coordinate transformation is applied. The resulting state-space representation is given as:

$$\begin{aligned}\dot{\tilde{x}} &= \begin{bmatrix} 0_{2 \times 2} & I_2 & 0_{2 \times 2} \\ \tilde{A}_{s,21} & \tilde{A}_{s,22} & 0_{2 \times 2} \\ 0_{2 \times 2} & 0_{2 \times 2} & \tilde{A}_{s,33} \end{bmatrix} \tilde{x} + \begin{bmatrix} 0_{2 \times 2} \\ \tilde{B}_{s,2} \\ \tilde{B}_{s,3} \end{bmatrix} u, \\ y &= [0_{2 \times 2} \quad \tilde{C}_{s,2} \quad \tilde{C}_{s,3}] \tilde{x},\end{aligned}\quad (9)$$

where the block matrices are described in the appendix.

The controllability matrix [5] is given by $M_c = [B \ AB \ \dots \ A^5 B]_{(\tilde{A}_s, \tilde{B}_s)}$ and the evaluation of its rank results $\text{rank } M_c = 4$. Therefore, according to the Kalman rank condition for controllability (KRCC) the system (9) is not controllable, since the dimension of the state vector is $\dim \tilde{x} = 6$. The non-controllable states of \tilde{x} are the position s and the orientation ψ .

Thus, a new coordinate transformation $z = T_{C\bar{C}}\tilde{x}$ is defined, such that $T_{C\bar{C}} = (T_C, T_{\bar{C}})$ is a basis for \mathbb{R}^6 , furthermore the columns of T_C form the basis for the controllable subspace, $\dim T_C = 6 \times 4$ and $\dim T_{\bar{C}} = 6 \times 2$. The state-space representation becomes

$$\begin{aligned}\dot{z} &= \begin{bmatrix} A_C & A_{C\bar{C}} \\ 0 & A_{\bar{C}} \end{bmatrix} z(t) + \begin{bmatrix} B_C \\ 0 \end{bmatrix} u(t), \\ y &= [C_C \quad C_{\bar{C}}] z(t),\end{aligned}\quad (10)$$

where, as a consequence of the definition, the state vector $z = (z_C, z_{\bar{C}})^T$ is clearly divided into two parts, namely $z_C =$

$(\theta_3, \dot{s}, \dot{\theta}_3, \psi)^T$ denotes the controllable states, while $z_c = (s, \psi)^T$ contains the uncontrollable ones.

The LQ strategy is elaborated by using the controllable subsystem (A_c, B_c) . The weighting matrices $Q = \text{diag}(Q_{ii})$ and $R = \text{diag}(R_{jj})$ were defined based on the Bryson's rule, where $Q_{11} = (15 \cdot \pi/180)^{-2}$, $Q_{22} = (0.08)^{-2}$, $Q_{33} = (50 \cdot \pi/180)^{-2}$, $Q_{44} = (50 \cdot \pi/180)^{-2}$ and $R_{11} = R_{22} = 3^{-2}$ were chosen. Solving the CARE the optimal control gain is

$$K^s = \begin{bmatrix} -1.75 & -1.26 & -0.2 & -0.61 \\ -1.75 & -1.26 & -0.2 & +0.61 \end{bmatrix}, \quad (11)$$

while the reference tracking matrices are

$$N_x^s = \begin{bmatrix} -0.41 & 0 \\ 1 & 0 \\ 0 & 0 \\ 0 & 1 \end{bmatrix}, \quad N_u^s = \begin{bmatrix} 4.28 & -0.37 \\ 4.28 & +0.37 \end{bmatrix}. \quad (12)$$

B. Kalman filtering

The Kalman filter is used to estimate the tilt angle θ_3 of the inner body (second element of \tilde{x}). Since the accelerometer measures the projection of gravity vector onto its axes, the angle is given by $\theta_{3,acc} = \text{atan}\left(\frac{a_y}{a_x}\right)$ [26]. Unfortunately, $\theta_{3,acc}$ is very noisy, in the most control methods it cannot be considered as an accurate derived quantity at high frequency rates of rotation because the accelerometer measures both the static acceleration of the gravity and the dynamic acceleration of the robot as well. Thus, it is common to consider the gyroscope and accelerometer sensors as a noisy linear system and use the Kalman filter to estimate the state vector. The corresponding state-space equation is given as:

$$\begin{aligned} \xi_{k+1} &= \begin{bmatrix} 1 & -1/f_s \\ 0 & 1 \end{bmatrix} \xi_k + \begin{bmatrix} 1/f_s \\ 0 \end{bmatrix} \rho_k + w_k \\ \gamma_k &= [1 \quad 0] \xi_k + z_k, \end{aligned} \quad (13)$$

where the state vector $\xi = (\theta_3, \tilde{u})^T$ consists of the inclination angle θ_3 [rad], and the bias of the gyroscope \tilde{u} [rad/s]. Furthermore, the input of the linear system is the angular velocity $\rho = \dot{\theta}_3$ [rad/s] (measured by the gyroscope), while the output of the system is the derived angle $\gamma = \theta_{3,acc}$ [rad] from the pure accelerometer measurements. The covariance matrices that characterize the measurement and state noises were defined based on offline measurements.

C. The LQG control strategy

According to the separation principle, the LQG control strategy is elaborated as follows. Around the stable equilibrium point the state feedback $u_k = -K(\hat{\theta}_3, \dot{s}, \dot{\theta}_3, \psi)$ ensures asymptotic stability of the closed loop system, where $\hat{\theta}_3$ denotes the Kalman filter based estimation of the tilt angle of the inner body and the optimal control gain K is defined by (11). The detailed control structure is depicted in Figure 2.

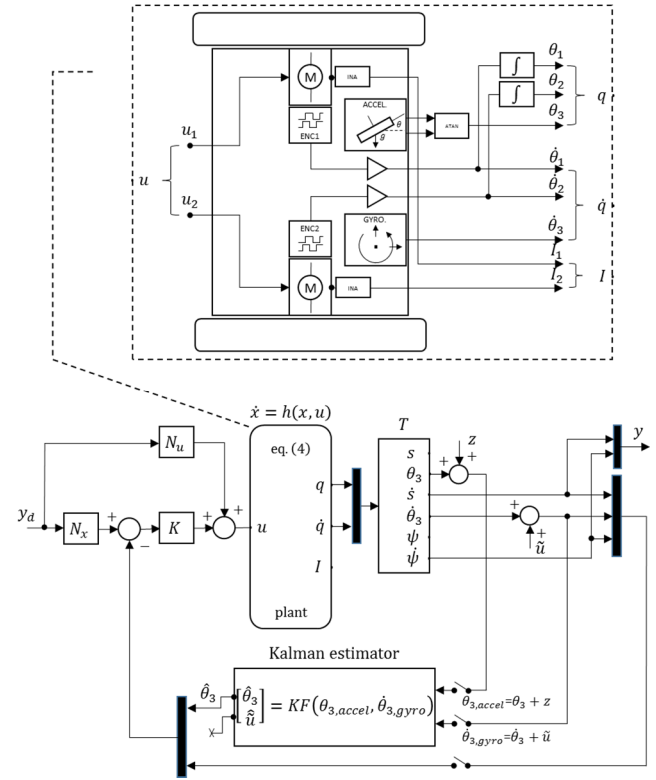


Figure 2. Detailed structure of the LQG control strategy.

VI. ELABORATION OF THE FUZZY CONTROL STRATEGY

The elaboration of the fuzzy control strategy consisted of defining the fuzzy logic controllers and a control scheme that satisfies the requirements of the anti-sway speed controller of the robot. This procedure was started by aggregating the deductions related to the behavior of the dynamical system using human common sense. The investigation resulted a control scheme that consists of three cascade-connected FLCs (hereinafter FLC1, FLC2, and FLC3). The control structure is depicted in Figure 3 [19].

FLC1 ensures the speed control of the robot. The input of the controller is the speed error $e_v(i) = v_d(i) - v(i)$, while the output is the variation $\Delta u_v(i)$ of the control voltage $u_v(i)$. An integrator is attached to the output of the controller, therefore, a PI-type FLC has been defined with the fuzzy rules defined in Table II, where the antecedent is e_v . Both the ranges of the input and output variables, and the membership functions are depicted in Figure 4. For the defuzzification of the output fuzzy set, the weighted average method has been chosen, therefore, the crisp control voltage u_v for the speed control of the robot is defined as:

$$u_v(i) = u_v(i-1) + \frac{\sum_{j=1}^3 \mu^j(e_v(i)) \cdot \gamma^j}{\sum_{j=1}^3 \mu^j(e_v(i))}, \quad (14)$$

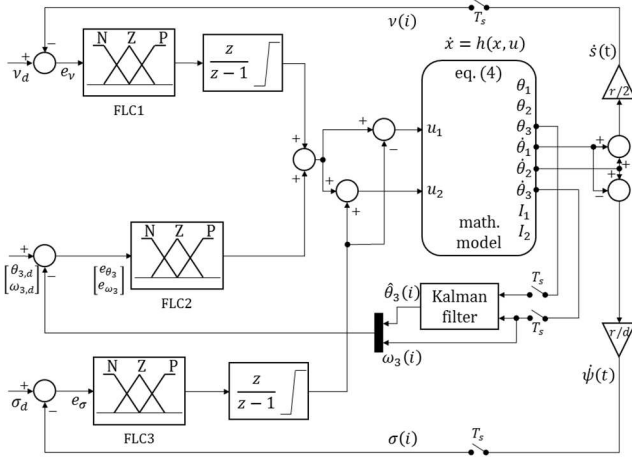


Figure 3. Block diagram of the fuzzy control scheme.

where $\mu^j(\cdot)$ returns the membership degree of the antecedent $e_v(i)$ related to the j -th-rule, and γ^j is the singleton consequent.

FLC2 is responsible for the suppression of the resulting inner body oscillations. The inputs of the controller are the error of the oscillation angle $e_{\theta_3}(i)$ and its derivative $e_{\omega_3}(i)$, while the output is the control voltage u_{θ_3} that shall be applied in order to decrease the acceleration of the robot. By decreasing the acceleration, the inner body oscillation is suppressed. FLC2 works as a PD-type fuzzy controller, whose fuzzy rules are indicated in Table II (the antecedents are the errors e_{θ_3} and e_{ω_3}). The universes of discourse of the input variables are depicted in Figure 4. The crisp output of the controller is calculated using the weighted average method:

$$u_{\theta_3}(i) = \frac{\sum_{j=1}^9 \min(\mu^j(e_{\theta_3}(i), e_{\omega_3}(i))) \cdot \gamma^j}{\sum_{j=1}^9 \min(\mu^j(e_{\theta_3}(i), e_{\omega_3}(i)))}. \quad (15)$$

Finally, FLC3 ensures the yaw rate control of the robot. The input of the controller is the yaw rate error $e_\sigma(i) = \sigma_d(i) - \sigma(i)$, while the output is the variation $\Delta u_\sigma(i)$ of the compensation voltage $u_\sigma(i)$. Similarly to FLC1, a PI-type fuzzy logic controller has been defined, whose fuzzy rules and membership functions are given in Table II and Figure 4, respectively. The crisp output of FLC3 is given as:

$$u_\sigma(i) = u_\sigma(i-1) + \frac{\sum_{j=1}^3 \mu^j(e_\sigma(i)) \cdot \gamma^j}{\sum_{j=1}^3 \mu^j(e_\sigma(i))}. \quad (16)$$

The control voltages of the motors can be identified based on Figure 3.

$$\begin{aligned} u_1 &= u_v + u_{\theta_3} - u_\sigma \\ u_2 &= u_v + u_{\theta_3} + u_\sigma \end{aligned} \quad (17)$$

The membership functions related to all control variables were chosen with triangular shapes. For the inputs and outputs of every FLC three membership functions were selected uniformly distributed across their universes of discourse (see Figure 4). Table III summarizes the inference mechanism of all the employed FLCs, while the fuzzy rules for the PD-type and PI-type FLCs are shown in Table II.

VII. SIMULATION RESULTS

The simulation of the proposed control strategies was done in MATLAB Simulink environment. The fuzzy logic controllers were designed by the help of the Fuzzy Logic Toolbox of MATLAB. The simulation results of the closed loop behavior is depicted in Figure 5.

From the top, the first is the linear speed \dot{s} of the robot, the second is the yaw rate $\dot{\psi}$, the third is the resulting oscillation θ_3 of the inner body, while the last one is the applied voltage to the motors. The following reference signals were applied:

- $v_d = \{0.4, 0, -0.2, 0\}$ [m/s],
- $\sigma_d = \{0.5, 0, -1.2, 0\}$ [rad/s].

TABLE II. RULE BASE OF PD AND PI-TYPE FLCS

PD-type				PI-type (+integrator)			
Consequent	Antecedent ₂			Consequent	Antecedent		
	N	Z	P		N	Z	P
Antecedent ₁	N	P	P	Z	P	Z	N
Z	P	Z	N	N	N	N	N
P	Z	N	N	N	N	N	N

TABLE III. PROPERTIES OF THE FLCS

AND method	OR method	Implication	Aggregation	Defuzification
MIN	MAX	MIN	MAX	Weighted average

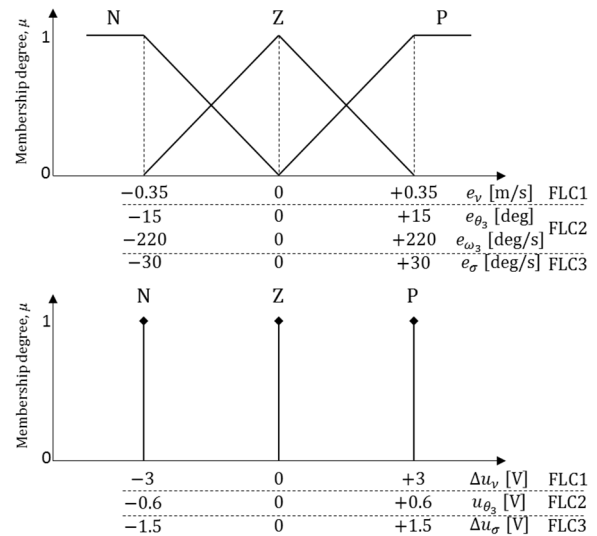


Figure 4. Membership functions of the employed FLCs.

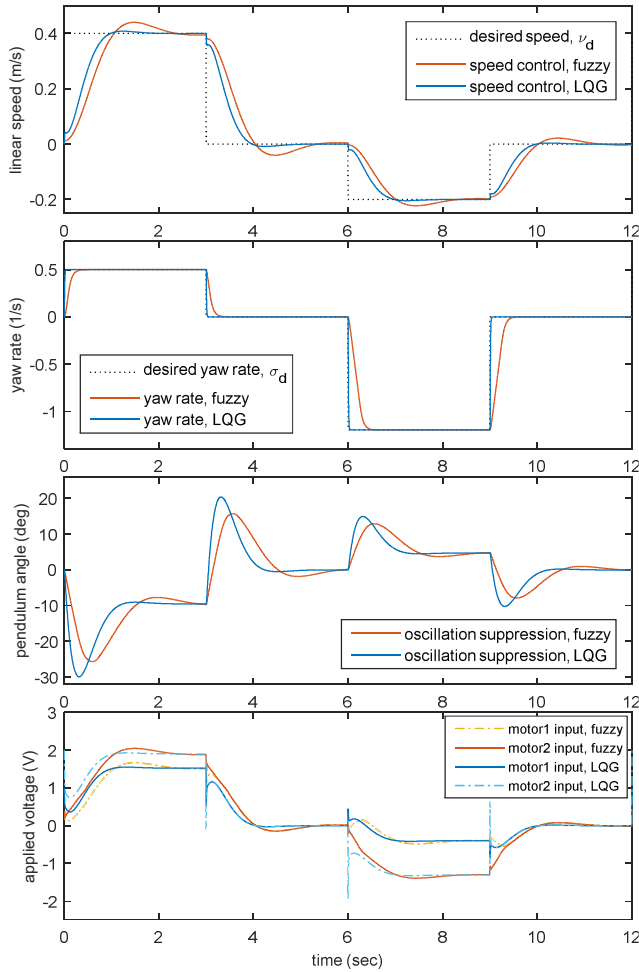


Figure 5. Closed loop behavior of the plant using the elaborated controllers (Simulation results).

The simulation results show that both the LQG control strategy and the cascade-connected fuzzy control scheme stabilized the dynamical system. It can be seen that the elaborated controllers simultaneously ensure the speed control (reference tracking performance is given in the first two subplots from the top of the figure) and the suppression of the inner body oscillations (third subplot). The dynamics of the plant was sampled at fixed $f_s = 100 \text{ Hz}$, which equals to the sampling frequency of the applied sensors.

VIII. IMPLEMENTATION RESULTS

The control algorithm was coded in C language. MCU2 was programmed to work as an inertial measurement unit (IMU). Its main task is to read the sensor data (from accelerometer and gyroscope through SPI peripheral), and send a package consisting of $\theta_{3,acc}$, $\dot{\theta}_3$, and $\hat{\theta}_3$ to MCU1 continuously in every $T_s = 10 \text{ ms}$, where $\theta_{3,acc}$ indicates the inclination angle (determined based on the pure accelerations measured by the accelerometer), $\dot{\theta}_3$ denotes the angular velocity of the pendulum (measured by the gyroscope), while

$\hat{\theta}_3$ indicates the Kalman estimation of the inclination angle. MCU1 executes the chosen control algorithm based on the collected measurements. It receives the package $(\theta_{3,acc}, \dot{\theta}_3, \hat{\theta}_3)$ from MCU2 and extends it with the instantaneous position and velocity of the robot (s, \dot{s}) based on the measurements collected from the incremental encoders. Once the measurements are updated, the chosen control algorithm updates the duty cycle of the PWM generator. Furthermore, the measurements are sent through a Bluetooth module with the frequency $f_s = 100 \text{ Hz}$. A GUI written in MATLAB records the measurements.

Regarding the LQG control, the calculated optimal feedback gains (11) and reference tracking matrices (12) have been directly used for the calculation of the control voltages by weighting the measurement results. The implementation of the FLCs was based on the fuzzy surfaces, which define the crisp output as a function of the input variables. Therefore, three look-up table has been stored in the flash memory of the MCU, and the control voltage has been defined by searching in these tables based on the instantaneous measurements.

The control performances are depicted in Figure 6. From the top, the first is the linear speed of the robot \dot{s} , the second is the yaw rate ψ , the third is the angle θ_3 of the inner body, while the last one shows the applied voltages. It can be seen that both implemented control strategies successfully suppressed the oscillation of the inner body and ensured the speed control of the robot as well. In the experiment, the desired speed and yaw rate has been set to 0.4 m/s and 3 rad/s , respectively (dotted lines in Figure 6). In the next section, the control performances will be qualified by defining different error integral formulas and a comparative assessment will be given based on the simulation and measurement results.

IX. COMPARISON OF THE CONTROL STRATEGIES

For the comparison of the elaborated control strategies both the transient responses and the overall control performance has been analyzed as well. The comparison was based on the closed loop behavior in time domain. For the quality measurement of reference tracking and suppression of inner body oscillations four different error integrals have been evaluated, namely these measures are the Sum of absolute errors (SAE), Sum of square errors (SSE), Sum of discrete time-weighted absolute errors (STAE), and the Sum of discrete time-weighted square errors defined by (18) and (19), respectively:

$$\text{SAE}(e) = \sum_i^N |e(i)|, \quad \text{SSE}(e) = \sum_i^N e(i)^2, \quad (18)$$

$$\text{STAE}(e) = \sum_i^N t(i)|e(i)|, \quad \text{STSE}(e) = \sum_i^N t(i)e(i)^2. \quad (19)$$

In (18) and (19), N denotes the length of the measurement, and e defines the error, which is the difference of the desired speeds and the actual speeds ($e = e_v$ or $e = e_\sigma$) in case of

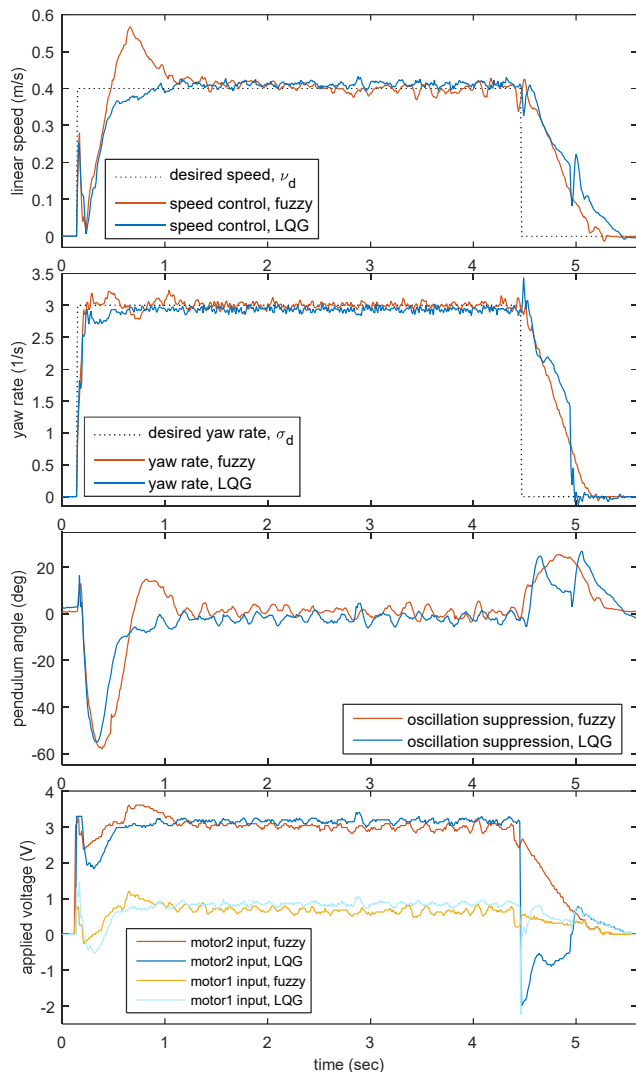


Figure 6. Control performances of the implemented LQG and fuzzy control strategies (Measurement results).

reference tracking, while in case of the suppression of the inner body oscillation $e = e_{\omega_3} = -\omega_3$ (since the desired rate of oscillation is zero, see Section IV). It was important to evaluate these quality-measuring expressions, because the results of the evaluation will form the initial fitness function values of the optimization of the fuzzy controllers in the next step of the investigation.

Based on the simulation and implementation results the qualitative characteristics of the elaborated controllers were summarized. The summary is given in Table IV, where T_{rise} indicates the rise time, $T_{5\%}$ denotes the settling time and ovs. is used for the abbreviation of overshoot. According to the simulation results, the LQG control strategy provided faster closed loop behavior with smaller reference tracking overshoot. From Table IV, it can also be read that the elaborated fuzzy scheme satisfies the control requirements with much bigger overshoot (0.036 m/s at 0.4 m/s reference speed), and due to the PI-type controllers it provides less

TABLE IV. CHARACTERISTICS OF THE CONTROLLERS

	Speed control of the robot			
	Simulation		Implementation	
	LQG	FUZZY	LQG	FUZZY
T_{rise} (s)	0.73	0.9	0.38	0.27
$T_{5\%}$ (s)	0.82	1.78	0.38	0.83
ovs. ($\frac{m}{s}$)	0.0083	0.036	0.018	0.14

	Suppression of the inner body oscillations			
	Simulation		Implementation	
	LQG	FUZZY	LQG	FUZZY
ovs. ($^{\circ}$)	29.9	25.6	52.7	56.3
$T_{5\%}$ (s)	0.85	1.19	0.71	0.91

aggressive closed loop behavior than the linear controller. Regarding the suppression of the inner body oscillations, both controllers performed the task similarly; the overshoot (e.g., maximum oscillation angle) was between 25-30 degrees.

These simulation results well predicted the outcome of the comparison related to the implemented controllers. The measurement results also proved that the LQG control strategy ensured faster system response and smaller overshoots. Regarding the fuzzy speed controller, the big overshoot is quite conspicuous (measurement results in Figure 6), and also, slower settling time characterizes the weaker performance of the fuzzy control scheme. Both realized controllers successfully suppressed the inner body oscillations with similar quality (e.g., the maximum overshoot was around 55 degrees).

According to the figures, it can be concluded that more satisfying control performance was achieved by the LQG control technique. The reason of the modest performance of the elaborated fuzzy control scheme could have different sources. It is important to mention that the realized controllers are the results of intuitive control design steps, meaning that the linear controller has been defined by selecting the Q and R weighting matrices (and taking into account the plant dynamics), while the inference mechanism of fuzzy control has been defined by the selected membership functions and rules. Moreover, it shall be kept in mind that the derived mathematical model (4) has not been validated, since the nominal (or calculated) values of inertia related (inertia matrix, center of mass) and electrical parameters (such as the resistance of inductance of the motor) that characterize the robot were used in the development procedure. The result of the not validated mathematical model can also be seen in Table IV, since we got significant differences between the simulation and implementation results. In fact, it was expected that the performance of the realized controllers will differ from the simulation results since the design procedure of the LQG control takes into account the mathematical model as a constraint equation (which is only approximately known), ultimately this difference led the system to a better closed loop behavior.

The evaluation of the quality measurement formulas (18) and (19) are summarized in Table V. The outcome of the evaluation results concludes controversy, since according to the calculated error integrals, the better overall control

TABLE V. QUALITY MEASUREMENT NUMBERS

Fuzzy control				
	e_v	e_σ	e_{ω_3}	$\log_{10} \Pi$
SAE	30.4780	128.7299	$4.2689 \cdot 10^3$	7.2240
SSE	6.5300	218.3223	$1.1638 \cdot 10^5$	8.2199
STAE	85.6093	512.2402	$9.4892 \cdot 10^3$	8.6192
STSE	20.3829	955.1933	$1.6724 \cdot 10^5$	9.5127

LQG control				
	e_v	e_σ	e_{ω_3}	$\log_{10} \Pi$
SAE	30.8451	150.3294	$3.7218 \cdot 10^3$	7.2370
SSE	6.9708	265.7726	$8.0833 \cdot 10^4$	8.1754
STAE	101.2168	581.9903	$9.1477 \cdot 10^3$	8.7315
STSE	23.8399	$1.169 \cdot 10^3$	$1.2966 \cdot 10^5$	9.5579

performance is provided by the fuzzy control scheme. The last column of Table V indicates that according to the SAE, STAE, and STSE quality measurement formulas the realized fuzzy control scheme results smaller aggregated error values. The rows of Table V define the chosen error integral formula, while the first three columns define the aggregated error value related to the errors e_v , e_σ and e_{ω_3} . The overall aggregated error value has been defined by multiplying the sub-aggregated error values, for example, in case of SAE:

$$SAE_{\text{overall}} = \log_{10} \prod_{e \in \{e_v, e_\sigma, e_{\omega_3}\}} SAE(e). \quad (20)$$

Therefore, the ultimate outcome of the comparison is that the LQG control strategy provided better transient system responses, however, the better overall control performance was achieved by the cascade-connected fuzzy control scheme. Through this analysis, we could see that approximate reasoning and the heuristic knowledge oriented development gave satisfying control performances. This suboptimal control solution can be further investigated and improved by using the quality measurement formulas (18) and (19) in an optimization procedure. In this optimization procedure, both the shape of the membership functions and their ranges could be optimized for a better overall control performance.

X. CONCLUSION AND FUTURE WORK

In this paper, LQG and fuzzy control strategies were elaborated for a two-wheeled mobile pendulum system. The elaborated control strategies successfully ensured the speed control of the robot and the stabilization of the inner body oscillations as well. The control performances were tested both in simulation environment and on the real robot. The comparative assessment has been given based on real-time behavior of the system, where the LQG control strategy provided faster system responses, however, the elaborated fuzzy control scheme ensured better overall control performance. These experiments form our initial results in the investigation of the control performances of different optimized modern control methods. Future work will involve the identification of the unknown parameters of the robot, since it was seen that the approximately known mathematical model significantly influenced the final outcome of the

investigation. Furthermore, the future research work will focus on the validation of optimized control strategies, where the defined quality measurement functions could lead the system to a better optimum.

ACKNOWLEDGMENT

We acknowledge the financial support of this work by the Hungarian State and the European Union under the TAMOP-4.2.2.D-15/1/KONV-2015-0002 project entitled "Development of Smart technologies for High-tech industry".

APPENDIX

The Lagrange function of the system:

$$\begin{aligned} \mathcal{L} = \sum_{i=1}^2 & \left(\frac{3}{4} m_w r^2 + \frac{1}{8} m_b r^2 + \frac{l^2 r^2}{2d^2} m_b \sin^2 \theta_3 + \frac{1}{2} J_B \frac{r^2}{d^2} + \frac{1}{2} k^2 J_r \right) \dot{\theta}_i^2 \\ & + \sum_{i=1}^2 \left(\frac{1}{2} m_b l r \cos \theta_3 - k^2 J_r \right) \dot{\theta}_3 \dot{\theta}_i \\ & + \left(\frac{1}{4} m_b r^2 - \frac{l^2 r^2}{d^2} m_b \sin^2 \theta_3 - J_B \frac{r^2}{d^2} \right) \dot{\theta}_1 \dot{\theta}_2 \\ & + \left(\frac{1}{2} m_b l^2 + \frac{1}{2} J_A + k^2 J_r \right) \dot{\theta}_3^2 - 2m_w g r - m_b g (r - l \cos \theta_3). \end{aligned} \quad (A)$$

Elements of the inertia matrix $M(q) = (m_{ij})_{3 \times 3}$:

$$\begin{aligned} m_{11} &= \frac{3}{2} m_w r^2 + \frac{1}{4} m_b r^2 + k^2 J_r + \frac{l^2 r^2}{d^2} m_b \sin^2 \theta_3 + J_B \frac{r^2}{d^2}, \\ m_{22} &= m_{11}, m_{33} = m_b l^2 + J_A + 2k^2 J_r, \\ m_{12} &= m_{21} = \frac{1}{4} m_b r^2 - \frac{l^2 r^2}{d^2} m_b \sin^2 \theta_3 - J_B \frac{r^2}{d^2}, \\ m_{13} &= m_{23} = m_{31} = m_{32} = \frac{1}{2} m_b l r \cos \theta_3 - k^2 J_r. \end{aligned} \quad (B)$$

TABLE VI. NOTATION OF THE ROBOT PARAMETERS

Symbol	Name	Value [SI Unit]
r	Wheel radius	$3.15 \cdot 10^{-2}$
m_w	Mass of the wheels	$31.6 \cdot 10^{-3}$
l	Distance between the COG and the wheel axle	$8.36 \cdot 10^{-3}$
m_b	Mass of the inner body	$360.4 \cdot 10^{-3}$
d	Distance between the wheels	$177 \cdot 10^{-3}$
J_A	Moment of inertia of the inner body about the wheel axle \mathcal{A}	$81367 \cdot 10^{-9}$
J_B	Moment of inertia of the inner body about the axis \mathcal{B}	$574620 \cdot 10^{-9}$
k	Gear ratio	64
J_r	Rotor inertia	$0.12 \cdot 10^{-7}$
R	Terminal resistance	2.3
L	Rotor inductance	$26 \cdot 10^{-6}$
k_M	Torque constant	$2.05 \cdot 10^{-3}$
k_E	Back-EMF constant	$2.05 \cdot 10^{-3}$
b	Viscous friction coefficient between body - motor	$2.1 \cdot 10^{-5}$
f_v	Viscous friction coefficient between wheels - ground	$1.8 \cdot 10^{-4}$

The elements of $V(q, \dot{q}) = (v_1, v_2, v_3)^T$:

$$\begin{aligned} v_1 &= 2 \frac{l^2 r^2}{d^2} m_b \sin \theta_3 \cos \theta_3 \dot{\theta}_3 (\dot{\theta}_1 - \dot{\theta}_2) - \frac{1}{2} m_b l r \sin \theta_3 \dot{\theta}_3^2, \\ v_2 &= 2 \frac{l^2 r^2}{d^2} m_b \sin \theta_3 \cos \theta_3 \dot{\theta}_3 (\dot{\theta}_2 - \dot{\theta}_1) - \frac{1}{2} m_b l r \sin \theta_3 \dot{\theta}_3^2, \\ v_3 &= -\frac{l^2 r^2}{d^2} m_b \sin \theta_3 \cos \theta_3 (\dot{\theta}_1 - \dot{\theta}_2)^2 + m_b g l \sin \theta_3. \end{aligned} \quad (C)$$

The block matrices of equation (9):

$$\begin{aligned} \tilde{A}_{s,21} &= \begin{bmatrix} 0 & -0.08 \\ -136.5 & \end{bmatrix}, \tilde{A}_{s,22} = \begin{bmatrix} -25.9 & 0.8 \\ 2338 & -73.6 \end{bmatrix}, \\ \tilde{A}_{s,33} &= \begin{bmatrix} 0 & 1 \\ 0 & -56 \end{bmatrix}, \tilde{B}_{s,2} = \begin{bmatrix} 3 & 3 \\ -279.6 & -279.6 \end{bmatrix}, \\ \tilde{B}_{s,3} &= \begin{bmatrix} 0 & 0 \\ -73.9 & 73.9 \end{bmatrix}, \tilde{C}_{s,2} = \begin{bmatrix} 1 & 0 \\ 0 & 0 \end{bmatrix}, \text{ and } \tilde{C}_{s,3} = \begin{bmatrix} 0 & 0 \\ 0 & 1 \end{bmatrix}. \end{aligned} \quad (D)$$

REFERENCES

- [1] Á. Odry, E. Burkus, and P. Odry, "LQG Control of a Two-Wheeled Mobile Pendulum System," The Fourth International Conference on Intelligent Systems and Applications (INTELLI 2015), 2015, pp. 105-112, ISBN: 978-1-61208-437-4.
- [2] K. S. Tang, Kim Fung Man, Guanrong Chen, and Sam Kwong, "An optimal fuzzy PID controller," IEEE Transactions on Industrial Electronics, vol. 48, 2001, pp. 757 - 765, doi: 10.1109/41.937407.
- [3] L. A. Zadeh, "Fuzzy sets," Information and Control, vol. 8, 1965, pp. 338 - 353, doi: 10.1016/S0019-9958(65)90241-X.
- [4] H. B. Verbruggen and P. M. Bruijn, "Fuzzy control and conventional control: What is (and can be) the real contribution of Fuzzy Systems," Fuzzy sets and Systems, vol. 90, 1997, pp. 151 - 160, doi: 10.1016/S0165-0114(97)00081-X.
- [5] G. F. Franklin, J. D. Powell, and A. Emami-Naeini, Feedback Control of Dynamic Systems. Pearson Prentice Hall, 2014, ISBN: 978-0-13349-659-8.
- [6] A. Divelbiss and J. Wen, "Trajectory tracking control of a car-trailer system," IEEE Transactions on Control Systems Technology, vol. 5, 1997, pp. 269 - 278, doi: 10.1109/87.572125.
- [7] J.-K. Ji and S.-K. Sul, "Kalman filter and LQ based speed controller for torsional vibration suppression in a 2-mass motor drive system," IEEE Transactions on Industrial Electronics, vol. 42, 2002, pp. 564 - 571, doi: 10.1109/41.475496.
- [8] S. Jeong and T. Takahashi, "Wheeled inverted pendulum type assistant robot: inverted mobile, standing, and sitting motions," IEEE/RSJ International Conference on Intelligent Robots and Systems (IROS 2007), 2007, pp. 1932 - 1937, doi: 10.1109/IROS.2007.4398961.
- [9] S. Zhiyu and L. Daliang, "Balancing control of a unicycle riding," 29th Chinese Control Conference (CCC), 2010, pp. 3250 - 3254, ISBN: 978-1-4244-6263-6.
- [10] L. Yi-bo, L. Wan-zhu, and S. Qi, "Improved LQG control for small unmanned helicopter based on active model in uncertain environment," International Conference on Electronics, Communications and Control (ICECC), 2011, pp. 289 - 292, doi: 10.1109/ICECC.2011.6067810.
- [11] O. Araar and N. Aouf, "Full linear control of a quadrotor UAV, LQ vs H ∞ ," UKACC International Conference on Control (CONTROL), 2014, pp. 133 - 138, doi: 10.1109/CONTROL.2014.6915128.
- [12] D. McLean and H. Matsuda, "Helicopter station-keeping: comparing LQR, fuzzy-logic and neural-net controllers," Engineering Applications of Artificial Intelligence, vol. 11, 1998, pp. 411-418, doi: 10.1016/S0952-1976(98)00005-0.
- [13] T. Das and I. N. Kar, "Design and implementation of an adaptive fuzzy logic-based controller for wheeled mobile robots," IEEE Transactions on Control Systems Technology, vol. 14, 2006, pp. 501-510, doi: 10.1109/TCST.2006.872536.
- [14] C. S. Lee and R. V. Gonzalez, "Fuzzy logic versus a PID controller for position control of a muscle-like actuated arm," Journal of Mechanical Science and Technology, vol. 22, 2008, pp. 1475-1482, doi: 10.1007/s12206-008-0424-7.
- [15] I. Kecskés and P. Odry, "Optimization of PI and Fuzzy-PI Controllers on Simulation Model of Szabad(ka)-II Walking Robot," International Journal of Advanced Robotic Systems, 2014, doi: 10.5772/59102.
- [16] M. Santos, V. López, and F. Morata, "Intelligent fuzzy controller of a quadrotor," International Conference on Intelligent Systems and Knowledge Engineering (ISKE 2010), 2010, pp. 141-146, doi: 10.1109/ISKE.2010.5680812.
- [17] Cheng-Hao Huang, Wen-June Wang, and Chih-Hui Chiu, "Design and Implementation of Fuzzy Control on a Two-Wheel Inverted Pendulum," IEEE Transactions on Industrial Electronics, vol. 58, 2010, pp. 2988-3001, doi: 10.1109/TIE.2010.2069076.
- [18] Á. Odry, I. Harmati, Z. Király, and P. Odry, "Design, realization and modeling of a two-wheeled mobile pendulum system," 14th International Conference on Instrumentation, Measurement, Circuits and Systems (IMCAS '15), 2015, pp. 75-79, ISBN: 978-1-61804-315-3.
- [19] Á. Odry, E. Burkus, I. Kecskés, J. Fodor, and P. Odry, "Fuzzy Control of a Two-Wheeled Mobile Pendulum System," 11th IEEE International Symposium on Applied Computational Intelligence and Informatics (SACI 2016), 2016, pp. 99-104, ISBN: 978-1-5090-2380-6.
- [20] Appl-DSP. Video demonstration of the robot. [Online]. Available from: <http://appl-dsp.com/lqg-and-fuzzy-control-of-a-mobile-wheeled-pendulum> [Accessed: 28 May 2016].
- [21] A. Salerno and J. Angeles, "A New Family of Two-Wheeled Mobile Robots: Modeling and Controllability," IEEE Transactions on Robotics, vol. 23, 2007, pp. 169 - 173, doi: 10.1109/TRO.2006.886277.
- [22] B. Cazzolato et al., "Modeling, simulation and control of an electric diwheel," Australasian Conference on Robotics and Automation (ACRA 2011), 2011, pp. 1-10, ISBN: 978-0-9807-4042-4.
- [23] L. Sciacivico and B. Siciliano, Modelling and Control of Robot Manipulators. Springer-Verlag London, 2000, ISBN: 978-1-85233-221-1.
- [24] G. Welch and G. Bishop, "An Introduction to the Kalman Filter," Tech. Rep. TR '95-041, Department of Computer Science, University of North Carolina, USA, 2001.
- [25] Li-Xin Wang, A course in fuzzy systems and control. Prentice-Hall, 1997, ISBN: 0-13-540882-2.
- [26] STMicroelectronics, "Tilt measurement using a low-g 3-axis accelerometer," Application note AN3182, 2010.
- [27] T. E. Marlin, Process control: designing processes and control systems for dynamic performance. McGraw-Hill Companies, 1995, ISBN: 0-07-040491-7.